Microfluid Nanofluid (2015) 18:513–526
DOI 10.1007/s10404-014-1450-7

RESEARCH PAPER

Integrated micromixer for incubation and separation of cancer cells on a centrifugal platform using inertial and dean forces

Gerson R. Aguirre · Vitaly Efremov · Maria Kitsara · Jens Ducrée

Received: 10 April 2014 / Accepted: 20 June 2014 / Published online: 6 July 2014

Abstract In this article, we demonstrate for the first time the integration of a micromixer unit for the creation of a cancer cell–microbead complex, and an inertial flow unit for the detection and separation in a centrifugal platform. The two units work under different operational principles but both exploit the centrifugal pseudo-force. The units achieve a high level of binding efficiency and a mechanism for cell sorting and guiding with the established asymmetric inertial flow system, respectively. The design of the passive micromixer takes advantage of the centrifugal force in an orthogonal direction to create what has been termed "flipping" to increase chaotic advection in the unit by turning the microchannel contents 180° at each turn. Blood was spiked into the system to identify maximum operational range. In non-spiked samples, cancer cells (MCF7) and microbeads bind together to generate cell–bead complexes (MCF7-PS) with a binding efficiency of 97.1 %; however, blood-spiked samples of 2 % v/v blood content were found to have a separation of 92.5 %, which diminished further with increasing blood content (5 % v/v blood). Once the complexes enter the inertial flow unit under these conditions, it remains in high operational flow-focusing standard with up to 98.7 % ± 1.4 of the introduced cancer cells reaching the designated outlet; for both units, unpaired statistical t tests show $P < 5$ with 95 % confidence level. This integration allows for the positive detection of cancer cells with reactive epitopes while the increased complex averaged size of cancer cell–microbeads standardizes the flow rate required for size-based flow-focusing. It can also be optimized for negative selection or multivariate detection of different cell biomarkers by enhancing sedimentation forces.

Electronic supplementary material The online version of this article (doi:10.1007/s10404-014-1450-7) contains supplementary material, which is available to authorized users.

G. R. Aguirre (✉) · M. Kitsara · J. Ducrée
School of Physical Sciences, Dublin City University, Dublin, Ireland
e-mail: gersonaguirre@gmail.com

G. R. Aguirre · V. Efremov · M. Kitsara · J. Ducrée
Biomedical Diagnostics Institute, National Centre for Sensor Research, Dublin, Ireland

1 Introduction

Medical diagnostics market enforced the development of the integrated biochips that enable us to perform complex biological and chemical procedures. Centrifugal platforms are easy to handle and can accommodate complex microfluidic networks; therefore, such platforms have been extensively used in academic and industrial research settings (Siegrist et al. 2010; Cho et al. 2007; Abaxis.com 2013). A range of molecular and cellular assays have also been reported (Burger and Ducree 2012; Park et al. 2013; SpinDx); however, the platform has found limited commercial success as a research or clinical tool. Conversely, lab-on-a-CD devices, or Biodiscs, for diagnostics have ample room for growth. Much attention has been placed on the development of the platforms for handling of biological fluids for the detection and diagnostics at the molecular level. Microfluidics has allowed miniaturization of macrosystems and thus the development of cheap and disposable platforms to purify and concentrate samples; however, little or no efforts have been placed on developing integrated systems that can effectively tackle efficient cell separation and their detection in this system with the exception of the spinout company SpinDxTM. One of the

major obstacles for the integration of diagnostic devices is the optimization of the limited real estate on the disc. This entails an understanding of how the interplay of fluid-flow forces and architecture can enhance operation to reduce on-chip footprint area.

Rotational flow systems operate under some different general forces than pump-driven flows. Inertia of fluid is one advantage that can be described by the pressure head and by the generation of counterflow drag force when the fluid is forced back, opposite to the centrifugal force. Some analogous dimensionless numbers that describe the physical phenomena of a centrifugal platform take into account these extra forces, such as Coriolis force, as a pressure gradient counter to the spin direction (used for mixing) and for inducing rotating counterflows such as Ekman layer. In curved channels, mixing is identified by the Dean number, while its analog in straight rotating systems is the Rossby number, which is the ratio of inertial to angular velocity determining the Coriolis force dominance (Boubnov and Golitsyn 1995).

1.1 Cell sorting

Cellular morphology has been reported to develop therapeutic understanding of several diseases (Pappas and Wong 2007); therefore, our ability to selectively sort the cells is critical. Systems for cell sorting are available, such as flow cytometry, which relies on immunostaining fluorescence signals from a large number of cells to be sorted (FACS), but these are expensive and their inability to process complex biological matrix is the most notable disadvantage. FACS provides high-throughput for sample sorting and counting defined by surface markers and proteins. However, it does not allow negative selection of cells in same sample and requires thousands of cells for processing. Magnetically activated cell sorting (MACS) is a column-based separation system based on cell surface-marker binding with magnetic beads containing coating of its antibody. The operational principle is triggered when the cell–magnetic bead complex crosses the magnetic field pulling it to an alternate outlet. It is limited to single cell line separation as multivariate immunoactivation is not possible under magnetic activation (Chen et al. 2010; Hou et al. 2011). However, complexity and heterogeneity of biological samples, primarily blood, makes sorting a more difficult and expensive process (Morijiri et al. 2011). Hydrodynamic microfluidic-based cell sorting has also had great success (see Sect. 1.2), such as pinch flow-focusing (Levin and Giddings 1991), splitting and recombining flow (SPLITT) (Hansson et al. 2012), inertial microfluidics (Oakey et al. 2010; Kuntaegowdanahalli et al. 2009), and counterflow elutriation (Morijiri et al. 2010). The limits of these systems range from non-focusing to high precision sorting but lacking ability to handle heterogeneous sample. Centrifugal forces enhance sedimentation forces to affect particles with different densities (Joseph 2002) leading to multivariate analysis of different cells.

1.2 Inertial flow

The Segré-Silberberg effect demonstrates the lateral migration of particles in macroscale flows in undisturbed streamlines under inertial conditions. The equilibrium positions for neutral buoyant particles are obtained by the balance between wall and shear gradient effects (Oakey et al. 2010). Further studies of this phenomenon (Matas et al. 2009; Gossett and Di Carlo 2009; Humphry et al. 2010) showed the dependence of particle size and two components of lift forces to create an equilibrium position between the centerline and channel wall. The condition creates entrainment with regular spacing along the direction of flow (Humphry et al. 2010) requiring low numbers to prevent steric crowding, which interrupts single-band streaming. This control is perfect for performing the separation of cells in samples with few cells. Particle separation and blood fractionation are necessary and easily performed in centrifugal systems. Microchannels with accentuated curved structures using the Zweifach–Fung effect (Zhang et al. 2008), density gradient (Cell Search Johnson & Johnson), immunomagnetic selection (Kirby et al. 2012) have had limited success ranging from the lack of specificity, purity of content, and sample volume handling.

Curved inertial microchannels easily perturb flowing particles from unstable positions (Oakey et al. 2010; Kuntaegowdanahalli et al. 2009; Matas et al. 2009). They enhance the speed of lateral particle migration to stable equilibrium positions faster than linear channels under similar flow rates. Biological cells are notoriously heterogeneous in size, density, and shape leading to pernicious loss of intended cells for capture or unaffordable real estate. The seminal paper by Asmolov (1999) accounts for a particle density function in inertial lift-based mechanics that removes the buoyancy dependence of particles. This translates to the flow-focusing of a particle regardless of its density, while the focusing principle is still particle size-dependent requiring appropriate flow rates. Averaging of cell diameter to reach a stable focusing position regardless of flow rates would be extremely beneficial to handle samples with large size distributions.

1.3 Micromixer

Passive and active micromixers are generally the two types of mixers found in microfluidic systems (Capretto et al. 2011; Sudarsan and Ugaz 2006). To reduce mixing time and length, the fluid stream is usually split. The use of diffusional or chaotic advection usually requires an external

force to drive the mixing process. At these characteristic length scales, it is hard to promote contact between participant materials to create mass transport in passive systems, some of which have designed architectures such as fluid injection (Voldman et al. 2000), split and recombine (SAR) (Fang and Yang 2009), Y- and T-type flows (Kamholz et al. 1999; Wong et al. 2004), multilaminar layers (Hong et al. 2004), 3D structures (Vijayendran et al. 2003), and obstacle-driven laminar flow breakup (Stott and Toner 2010; Wang et al. 2002; Stroock et al. 2002) to achieve mixing. Attempts to overcome this difficulty by adding active energy systems have included the use of temperature (Tsai and Lin 2002), electrical field (Mugele and Baret 2005), acoustic fluid shaking (Yang et al. 2001), pneumatic-driven (Xin et al. 2011), and microstirrers (Lu et al. 2002). In rotational systems, Coriolis forces (Brenner et al. 2005), reciprocating flow mixers (Noroozi et al. 2009), and centrifugo-pneumatic siphoning (Godino et al. 2013) play crucial role in overcoming the aforementioned limitation. Centrifugal systems designed for the separation of blood are classical examples of a rotation-based microfluidic platform, which have mainly made use of a density gradient (Schaff and Sommer 2011) or RBC lysing to separate erythrocytes from target cells and concentrate samples or plasma extraction (Sollier et al. 2009).

The majority of these mechanisms have had varying levels of success, but a mixing unit for highly effective binding of microparticles to cells under high-throughput flows has not been demonstrated. Recently, a serpentine micromixer on a centrifugal system was utilized for biochemical assays (La et al. 2013). This design demonstrated effective mixing of a pH indicator (phenolphthalein) and NaOH solutions of a biochemical albumin assay. The first part of our integrated microfluidic system—the mixing unit—has similar serpentine structure as the later publication. However, differences are enhanced mixing created in our unit by a series of curved features along the channel and also variance in dimensionality. In our case, effective mixing of microparticles and cancer cells was achieved.

Under laminar conditions ($Re < 100$), straight channels do not create any mixing. Serpentine channels generate transverse flows with respect to the main flow that can produce chaotic advection (Stroock et al. 2002; La et al. 2013) and reduce mixing length. This design allows for Dean vortices to grow and perturb laminar flow. Under centrifugal forces, Eq. 1 demonstrates the theoretical sedimentation time for a spherical particle of defined density in liquid to reach the bottom of a tube which in our case is a channel.

$$t = \frac{18\eta}{\omega^2 r_p^2 \left(\rho_p - \rho_t\right)} \times \ln \frac{r_b}{r_a} \quad (1)$$

where ρ is the density of particle and liquid, η is the viscosity of liquid, ω is the angular velocity, r_a is the center of rotation where the meniscus of liquid starts, and r_b is the bottom of tube.

1.4 Integration

Previous attempts to integrate systems have been relatively successful; however, the focus has been on molecular mixing with magnetic particles relying on the induction of magnetic field for separation (Kirby et al. 2012; Jung et al. 2011). Our system consists of two distinct steps: creation of cancer cell complexes by mixing of the spiked sample with the immunoparticles, each solution with independent inlet, and separation of complexes by inertial flow. While both systems rely on profoundly different physical phenomena in the respective units, their architecture and integration while under centrifugal field makes this an advancement to integrated centrifugal systems. It is noteworthy mentioning that some of the mixers referenced have also been used to separate particles and blood.

The system described here possesses the ability to create chaotic advection and ordered particle entrainment within their respective units. The integrated system contains both a passive and active mixer (Dean and centrifugal forces) and an inertial flow-focusing unit for separation. Though the definition for active mixer includes an energy source for fluid activation, here the combination of the geometry and centrifugal field generate an additional mixing scheme. This scheme allows for maximizing interaction of cells and particles (ref Sect. 2.3). Here, mixing is an essential first step for immunoreactivity of particles to cancer cells for the ease of detection and conduction to proper flow-focusing positions. The use of high-throughput velocities is also necessary to handle large volumes. The method of the platform described here ranks amongst the least demanding in terms of design, fabrication, actuation, and instrumentation. It also allows for the detection and classification of cancer cells from blood.

2 Materials and experimental methods

2.1 Fabrication

Designs were made using SolidWorks 2012 SP2.0. The disc-shaped microfluidic device was fabricated using standard soft lithography by casting polydimethylsiloxane (PDMS) on a SU-8 photoresist mold. Briefly, SU-8 3025 (Microchem, MA, USA) was spin-coated onto a 5″ silicon wafer and baked on a level hot plate at 95 °C for 15 min. Subsequently, the wafer is exposed to UV light using a mask aligner (OAI 206 CE). Post-exposure bake was

performed at 95 °C for 3 min. Next, the SU-8 was developed and hard-baked for 10 min at 150 °C and silanized using octadecyltrichlorosilane (Sigma-Aldrich, IE) vapors for at least 4 h. Then, it was casted on the SU-8 mold and cured in a 70-C oven for 45 min. For the bottom seal, a PMMA disc of 1.5-mm thickness was spin-coated with PDMS. This thin film was prepared using 20:1 (w/w) ratio of base/curing agent, spun at 1,500 rpm for 30 s, degassed in a vacuum chamber for 30 min, and cured in a 70-C oven for 1 h. Two fluidic access inlets and three outlets were punched into the fluidic PDMS layer using a flat-tip needle. The two parts were treated with O_2 plasma (PDC-002 Harrick Scientific Corp. USA) for 5 min each and then were manually aligned and bonded at 70 °C for at least 4 h. The height of both the mixing (symmetric) and inertial (asymmetric) channels is $\sim$70 μm. The mixing channel's width is 150 μm with a total mixing area of 16.70 mm^2. The asymmetric unit contains 6–8 turns, and each turn consists of one small and one large turn with widths 350 and 650 μm, respectively.

2.2 Sample preparation

MCF7 breast cancer cells and anti-Epcam functionalized beads were used in the mixing system. MCF7 cells were cultured in 75-cm^2 flasks in DMEM medium (Sigma-Aldrich, MO, USA), with 10 % un-inactivated fetal bovine serum (FBS), 100 U/ml penicillin, and 100 μg/ml streptomycin. Culture was maintained at 37 °C with 5 % CO2. Harvesting of cells was carried out by incubation in 5 ml 0.25 % trypsin/0.1 % EDTA at 37 °C for 5 min followed by neutralization with 5 ml DMEM culture medium. Cells were centrifuged at 300×g for 4 min and resuspended in DMEM culture media.

Protocol for the functionalization of PS beads with MCF7 cell epitope was as follows. SuperAvidin-coated 15.27 μm PS beads ($\rho = 1.06$ g/mL) (1 % solids) purchased from Bangs Laboratory were washed with PBS buffer three times. Sedimentation was performed to remove supernatant and exchange buffer solutions. This was followed by the addition of 25 μl of Human EpCAM/TROP-1 biotinylated antibody (50 μg) anti-EpCAM (R&D Systems) to 400 μl SuperAvidin microbeads and incubated with rotation for 15 min at room temperature. Blood was extracted directly from healthy donors via finger-prick using 1.5-mm sterile lancets (BD Biosciences, NJ, USA). Protocol for MCF7 cells for the blood dilution is as follows: firstly, anticoagulant was added to blood (100 μl EDTA 60 mM in 900 μl of blood) and then the anticoagulated blood was diluted to 2 and 5 % v/v using the following buffer: 100 mM PBS, pH 7.4/0.05 mM EDTA.

The unit consisted of two adjacent inlets for the spiked blood sample and PS particle solution, separately. A 200:1 bead-to-cancer cell ratio was used in all experiments. The system was primed with buffer solution. Sample solutions were loaded into inlets containing sample holders, and angular velocity was set to 3.75 Hz. Final volume was 1.0 mL placed in 1-mL micropipette tips, acting as sample holders of PMMA, and cooked in place with 10:1 PDMS/curing agent mixture that was fixed in external inlets made. Live cells were diluted to obtain desired numbers ($\approx$1,050, 500, 250 cells) and were fluorescent-stained with NucBlue™ Live Cell Stain (Life Technologies, CA, USA) for 5 min, followed by three wash steps with PBS. All experiments were ran three times, $n = 3$. The same buffer medium was used for the priming of the channels before the introduction of sample. Micrographs were recorded in a microscope and post-processed using Fiji software.

2.3 Operational principle

The system presented here constitutes two integrated units that operate under the same centrifugal force field but have different physical operational principles. The integrated system consists of sequential (1) micromixer and (2) inertial asymmetric channels where the designs of both units make use of radial turns to achieve desired results. The mixing unit contains two inlets for separate input of biological sample and PS particle binding solutions. The pressure-driven flow is driven by an angular velocity = 3.75 Hz. This angular velocity allows for high binding of cancer cells and control of particle focusing induced by inertial flows (Kitsara et al. 2013) with percentages as high as 97 % while preventing sedimentation. The azimuthal channels provide a longer residence time and in this case of mixing due to the flipping mechanism. After the cells bind to the microbeads, the centrifugal force influences the trajectory of the complex creating entrainment at the beginning of the inertial channel shortening the lateral distance needed to achieve focusing inside the inertial channel.

The micromixer works on the principle of secondary flows generated by Dean flows to enhance particle and cell mixing. Symmetric sidewinding channels running along the azimuth direction of the disc with several rows (Fig. 1) with 5 "flipping" turns were placed to increase the dynamic mixing area. The orthogonal placement of the mixing channels allows, under the influence of the centrifugal force field, the 180° inversion of the direction of the particles away from the sedimentation path which we termed "flipping." The mechanism of particle trajectory turning on its axis at the end of each row is due to the centrifugal field being constantly orthogonal. This creates mixing of contents while flow continues along the serpentine channels preventing settling. The Archimedes (Ar)

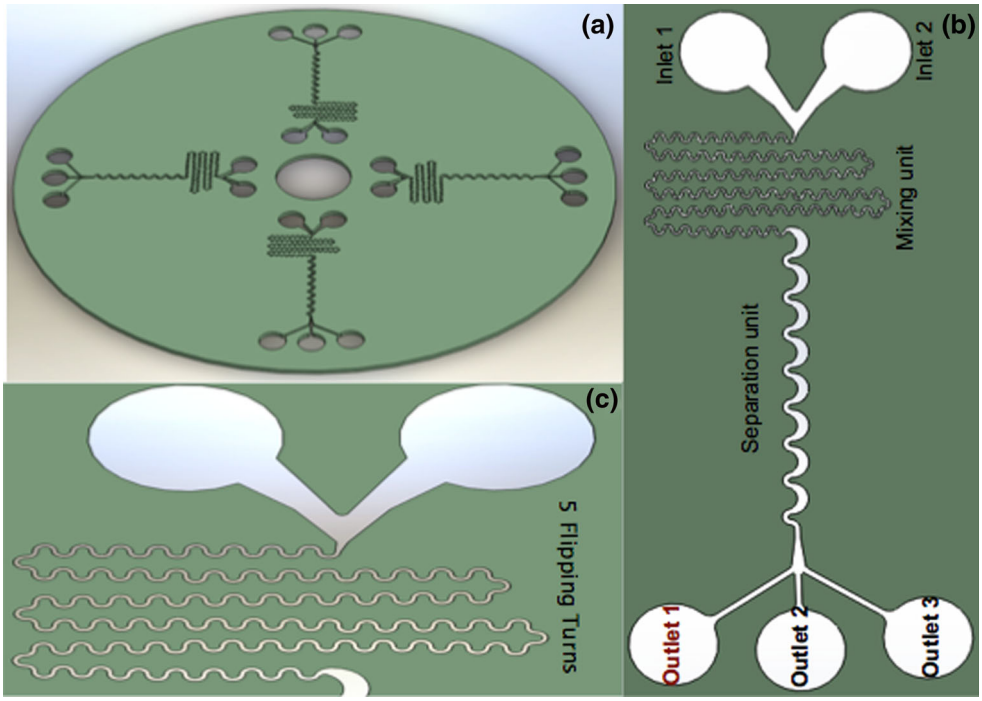

Fig. 1 **a** Schematic of integrated lab-on-a-disc system, **b** close-up of one of the four segments comprising disc. It identifies the two inlets, mixing unit and the connected inertial flow-focusing channel, **c** zoom in of mixing area depicting the five turns where flipping occurs in integrated disc which enhanced mixing

dimensionless number was used to determine the viability of particle buoyancy. It represents the ratio between buoyancy and inertial forces, which can be used to asses particle–fluid flow interaction. Flow transport here is natural convection-driven as $Ar = 4$, a condition where the density of an object relative to the liquid will sink or float. The combination of particle buoyant forces with secondary flows found in Dean forces provides binding of PS particles with biotinylated anti-EpCam to live MCF7 cancer cells.

The inertial asymmetric channel, which is connected radially outward to the micromixer, is used for focusing of the complex. This system was previously developed as a size-based particle filtration device. The lateral migration for a specific particle diameter is velocity-dependent in precise channel geometries (Gossett and Di Carlo 2009). With our sequential arrangement, the focusing is achieved at flow rates a fraction to that required by pump-driven systems (Oakey et al. 2010; Gossett and Di Carlo 2009). Since lift-based inertial microfluidics is not particle density-dependent, the small difference in densities do not obviate focusing. When blood is added to the system, the three outlet system allows for the determination of binding efficiency and defocusing due to steric hindrance. However, a high percent binding and focusing is still found in the system.

3 Results and discussions

In this work, we integrate two units that operate in flow-through mode. The two units operate continuously to maintain a high-throughput processing of two solutions: a solution with different percentages of blood-spiked with MCF7 cell numbers ranging from 1,050 to 250 and the 15-μm-diameter PS microbead solution. We take advantage of the centrifugal pseudo-force field to bind the epitope-specific PS particles to cancer cells. After the sample has been processed in the mixing unit, it enters the inertial flow channel for induced focusing of the created complex and the outlets for fractional sample collection for analysis.

3.1 Mixing unit

In addition to the mixing provided by Dean forces, the operational principle for this unit is the placement of the alternating sidewinding channels (Fig. 1) that cause what we have termed "flipping" to describe the behavior which we believe enhances binding. Under centrifugal force, an object will eventually sediment (Eq. 1).

However, in this design, while under fluidized conditions, the end of each row creates the 180° flipping direction of the contents and enhances mixing leading to chaotic advection.

This allows the mixing to restart at every turn and reduces the radial distance required to achieve proper mixing under laminar flow conditions. The unit contains a total number of five "flipping" turns.

To process the sample, an angular velocity of 3.75 Hz is used, which was determined in a prior work (Kitsara et al. 2013) where the particle focusing induced by the inertial force remains dominant over Coriolis force displacement

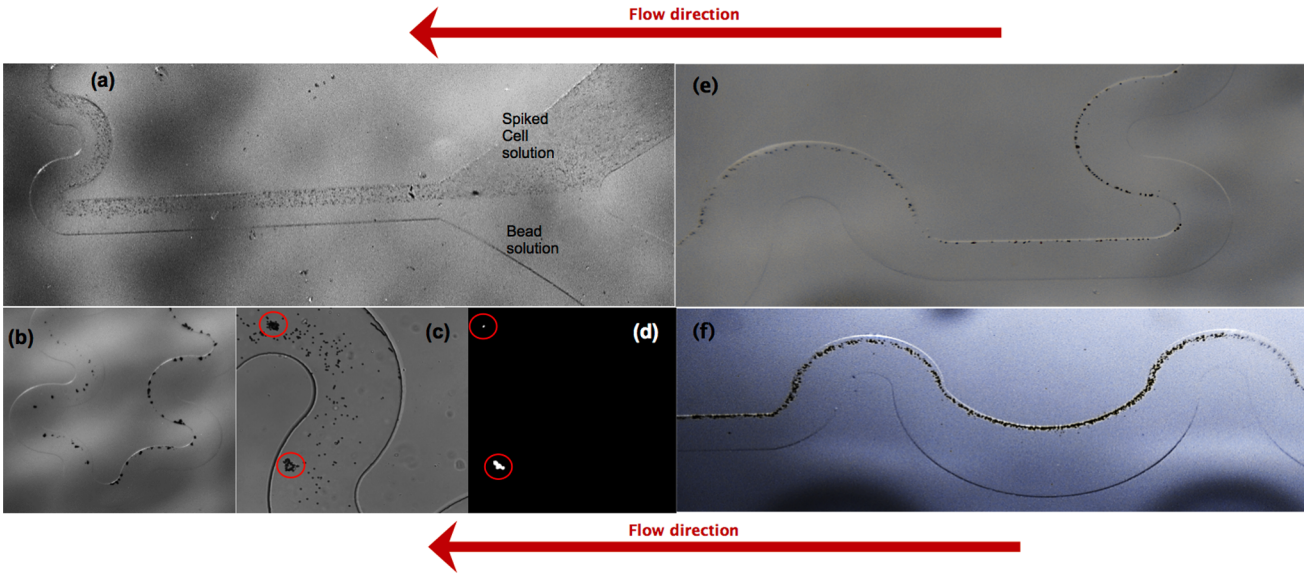

Fig. 2 Micrographs of integrated system. Mixing unit: **a** upstream section of the mixing unit processing blood-spiked and microbead solutions. Sample with no blood for clarity (**b**–**e**). **b** Notice the higher number of particles on bottom section of channel, whereas when channel configuration "flips" direction, the particles are more distributed in channel showing contributing to advection. This "flipping" of contents enhances the mixing mechanism. **c** Differential interference contrast and **d** fluorescence DAPI filter microscope images of the cells bound near end of mixing unit (indicated in *red circles*). **e** Entrance of complexes from mixer into inertial unit. Notice entrainment of particles. Inertial flow: **f** Single-band flow-focusing of a sample without blood in inertial channel. *Red arrows* show flow direction (color figure online)

of particles. The $Re_{av} = 11$, which is the average Reynolds number at this frequency, and the flow rate in the microfluidic channel can be scaled to $Q \sim d^4$. At these conditions, the flow is under natural convection and the buoyancy of particles and cells remains density-based. The densities of PS microspheres and cancer cells are close, thus allowing the centrifugal force field to affect their buoyancy similarly. To the left of Fig. 1 is a diagram of the lab-on-a-disc system and a single unit composed of two inlets, mixing unit, inertial unit, and three outlets. Outlet 1 is the designated outlet for all focused particles independent of binding. Figure 1c is a zoom in the mixing unit to identify the five mixing turns. These turns allow the solid contents of the solutions to undergo enhanced mixing due to the interplay of the centrifugal force, buoyancy, and secondary flows created by the curvature of the channels under pressurized flow.

To demonstrate the operation of the mixing unit, a micrograph of upstream mixing of a blood-spiked sample and microparticle solution is shown in Fig. 2a. For the clarity of visualization, micrographs of a sample without blood are shown in Fig. 2b–f. A (DAPI) DNA-stained cell bound by microparticles and its fluorescence shows the significant level of binding the mixing unit provides. These micrographs clearly show the creation of the complex of MCF7 cells to PS microbeads and their transition into the inertia flow unit.

As the complexes of cell and microbead move downstream of the micromixer, they start to align (Fig. 2e). It is also observed that this behavior forces flow-focusing of cells and particles at a lower flow rate (SI video 1) than theoretically expected systems (Oakey et al. 2010; Gossett and Di Carlo 2009) as shown in Fig. 2f. Previous reported values for Reynolds numbers (*Re*) for cell or particle focusing based on particle diameter are at least three times the *Re* achieved here (Matas et al. 2009). This is attributed to the effect of the sedimentation forces in the micromixer due to centrifugal field on the components. This is another advantage demonstrated over pump-driven microfluidic systems.

For efficiency comparisons, off-chip incubation experiments with blood were ran in a rotator. This was the control for the determination of binding efficiency of the mixing system in our experiments. The histogram in Fig. 3 shows the efficiency of the mixing system when compared with off-chip incubation with similar blood content. Off-chip incubation of MCF7 cells was shown to be highly efficient with 98.3 ± 1.7 % of bound cells to microparticles. All statistics were generated under a microscope. The data show that with decreased number of cancer cells, the system continued to have effective binding with a mean percentage range of 97.12 ± 1.9 % ($n = 3$) as even the maximum number of cells plus microbeads is still below the level of particle density for inertial self-ordering. A

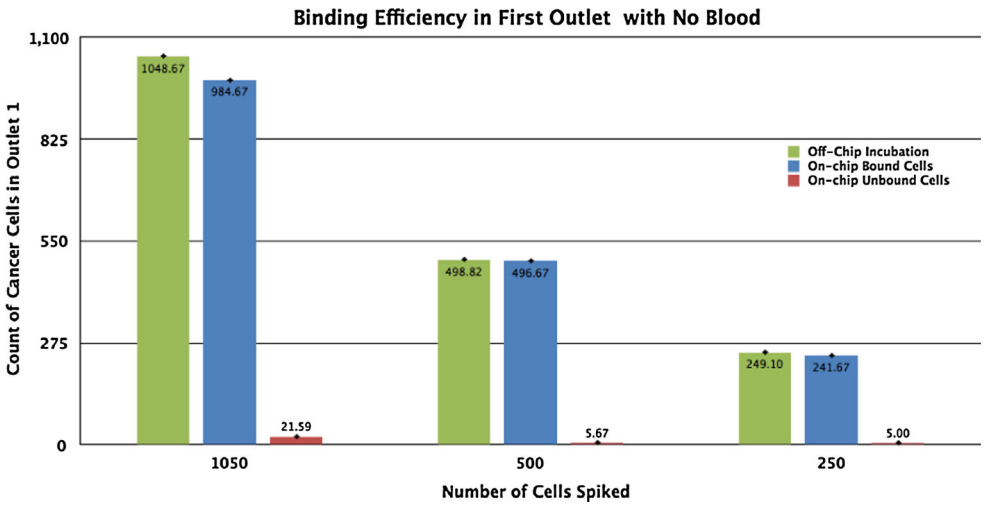

Fig. 3 Comparison of on-chip particle cell binding efficiency and off-chip incubation without blood (*green*) as number of MCF7 cells found in first outlet due to flow-focusing. When the system consists only of cells and microparticles (no blood), the on-chip binding efficiency is consistently very high (*blue*) with low number of unbound cells (*red*) (color figure online)

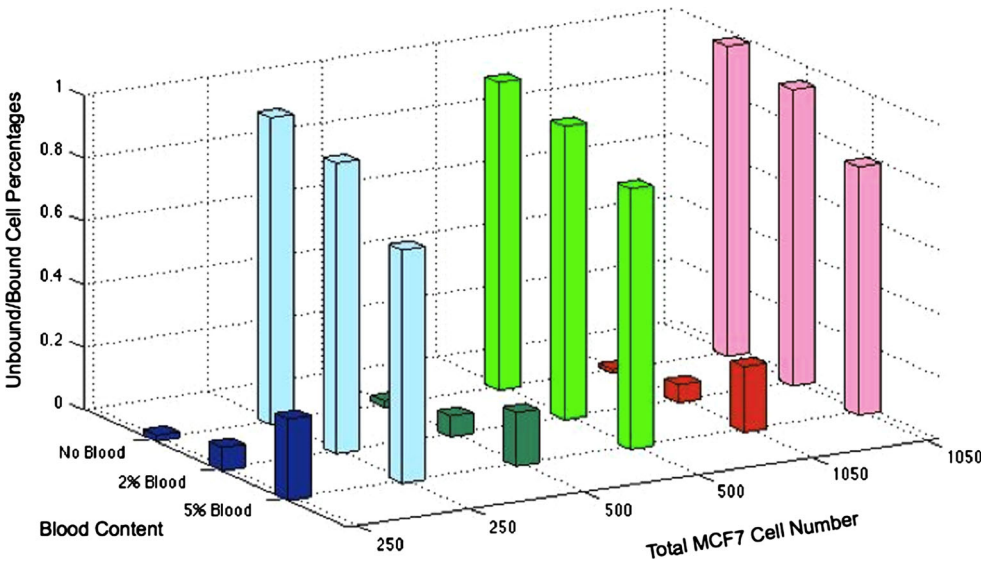

Fig. 4 Histogram of binding efficiency based on the number of cells (1,050, 500, 250) and changes in blood content in outlet 1. High binding efficiency is noticed for 2 % v/v blood content while for 5 % v/v content, a significant drop is noticed regardless of number of cancer cells in system. *Light colors* represent percentages of bound cell microparticle and *darker colors* unbound cell (color figure online)

t test value of 1.96 with $P < 0.05$ with differences considered significant at the 95 % confidence level for data with normal distribution was obtained. These results show that the mixing area provides adequate mixing of the components to high levels with standard errors within a very respectable range regardless of the number of targeted cells processed.

To find the limits of mixing efficiency, the content of blood-spiked was increased in the system. The percentage of the total number of cancer cells against the non-bound cells in outlet 1 was counted when different contents of blood were added. Blood contents of 2 and 5 % v/v were used but the number of spiked cells was kept constant. The histogram in Fig. 4 shows the consistency and reproducibility of binding at the lower content of blood; however, a significant drop in binding is seen when the content was increased to 5 % v/v blood content. An 94.2 % binding percentage is found in 2 % v/v blood content for 1,050 spiked cell samples, which decreased by about 15.1 % with the higher blood content, and it was more acute as the number of spiked cancer cell was lowered to 74.3 % measuring about 15.7 % difference with 250 MCF7 cells sample. The lowering in binding efficiency within the micromixer is due to steric hindrance from the content of blood added. As opposed to the forces in the inertial flow unit that are to create order, mixing is the process necessary for increased probability of MCF7 cells to meet PS microbeads.

The micrographs of a large processed sample in Fig. 5 shows high binding efficiency is still obtained with 2 and 5 % v/v blood. The complexes in blue circles show the high affinity, which for outlet 1 at 2 % v/v blood content it is shown to be pretty high, while the red circles are cancer cells that did not bind to the microbeads. The amount of blood was chosen to be within the working range of inertial microfluidics systems (Oakey et al. 2010; Gossett and Di Carlo 2009) to allow single flow-focused condition (SI

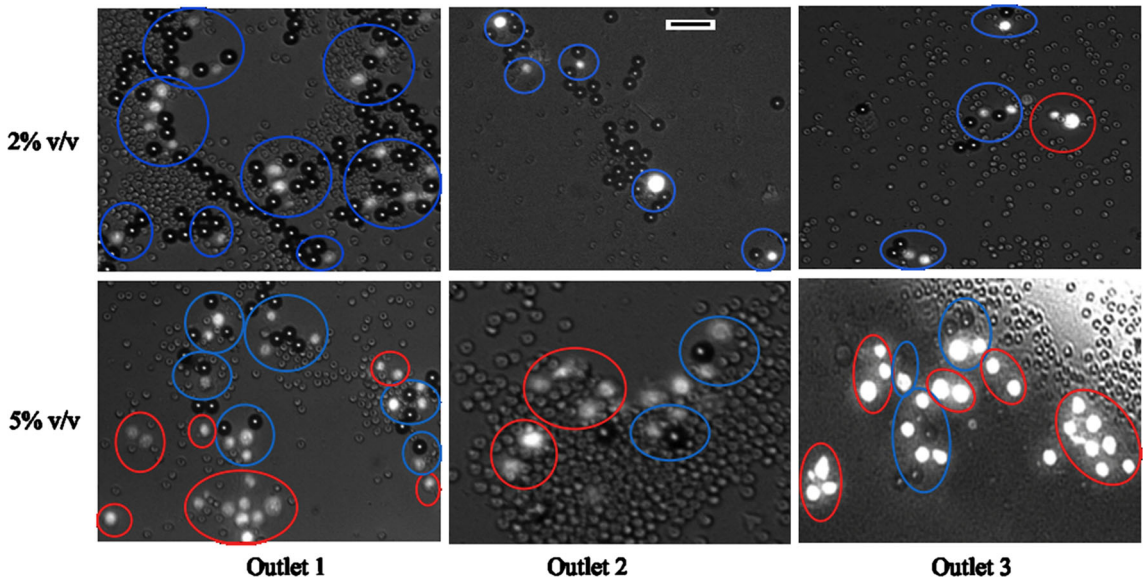

Fig. 5 Micrographs of sample of (MCF7-PS) cancer cell–microbead complexes for all three outlets with two different contents of blood in the system. *Top* notice the high binding of particles and cells (*blue circles*) while few are not bound (*red circle*). Outlet 1 with 2 % v/v blood content shows high binding efficiency. *Bottom* with blood content increasing to 5 % v/v, lower number of bound cancer cells to microbeads is found. *Scale bar* is 50 μm (color figure online)

video 2). This demonstrates that however robust the micromixer is, it is limited to low concentration of blood. Notwithstanding this limit, the integration with an inertial flow system for the separation of blood content requires a low number of constituent particles to achieve focusing. The distribution ratio of blood content was ~3:3:1 in each outlet from outlets 1–3, respectively.

The high binding efficiency demonstrated here by the micromixer is within a good limit and within operational range to achieve lateral movement for the inertial forces to be dominant. Experiments were done (data not shown) with wider channel dimensions (250 μm) but efficiency was not as high. This demonstrates there is a limit of mixing/binding efficiency in Dean flow channels due to the limited chaotic advection created in passive micromixers in wider channels.

3.2 Flow-focusing unit

The system contains three outlets that were used for fractional sample collection. Outlet 1 was designated as the dedicated direction for all particles as imposed by the lateral translation of particles in the inertial flow unit (Fig. 1). The other two were used to monitor the influence of the blood-spiked content on both the binding efficiency and focusing control. As shown in SI video 1, where a sample without blood was processed, the system shows the expected focusing of an inertial system within its operational limit. The behavior of addition of blood content to the spiked cell solution is investigated.

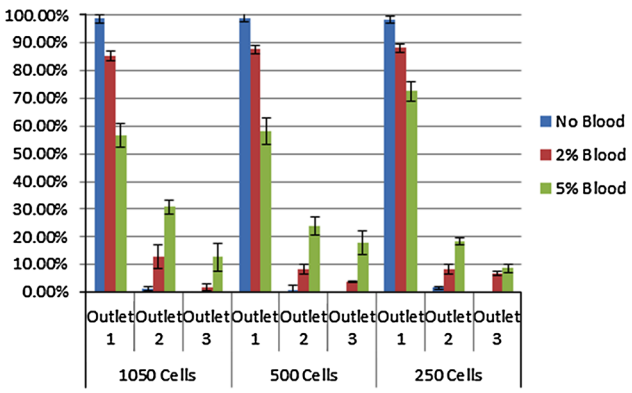

Fig. 6 Histogram showing percentage of cell–microbead complex based on blood concentration of MCF7 cells found in each outlet. High control of focusing is still shown with low content of blood. Steric effect of increased content is more pronounced, and deviation leads to less designated outlet focusing

In Fig. 6, the histogram shows the deviation from effective deterministic flow-focusing as a breakdown of the constituents found in each of the three outlets (SI video 3). The flow-focusing control drops to a dynamic range from 99.1 ± 1.3 to 98.4 ± 1.2 % standard error for outlet 1 with no blood based on MCF7 content. This drops to 56.5 ± 4.2 % with highest blood content (5 % v/v) and MCF7 (1,050) cell numbers. Samples ran with 5 % v/v blood content consistently showed higher random alignment in channel. Higher deviation is obtained due to steric effects and increased volume fraction beyond the dynamic range of inertial particle focusing allows systems (Gossett

and Di Carlo 2009). The low number of cells that enter the third outlet is still more random with 5.0 % standard error, an above acceptable error margin. However, when the 2 % v/v dynamic range in the inertial microchannels is maintained, the expected behavior is controlled and the guidance of the cell–microbead complex is obtained, which aids in the identification of cancer cells as well.

This effect was demonstrated also in our simulations, see below. As the movement of particles is perturbed to a position of equilibrium, the initial position in which they entered the channel will have an effect on how long it will take for them to reach the equilibrium position. This is made more complicated by the fact that the system is particle size-based to reach focusing. Meaning that an enlargement of the average complex diameter will reduce the required velocity to reach its equilibrium position but be displaced by the interaction with blood contents. When blood is introduced into the system, the steric effect is greater and deviates the trajectory of the complex from outlet 1. The statistics for this unit gave the same results as the mixing unit suggesting that the blood content is a parameter affecting the integrated system equally in both units.

With the need to utilize smaller sample volumes afforded by microfluidics, many diagnoses of biological diseases and conditions require a small cell count. The integrated system presented here shows the ability to allow detection of events that exhibit a Poisson distribution nature (Tibbe et al. 2007; Oakey et al. 2010). The size variance of biological and specially cancer cells, which may contain clusters of cells (Paterlini-Brechot and Benali 2007), has been an obstacle for separation using hydrodynamic forces. However, obtaining the proper flow rates for size-based inertial flow-focusing is easier with the cell–microbead complex formation as the averaged size is increased requiring lower speeds and the initiation of entrainment standardizes the flow rate to provide proper mixing, as is the case here.

3.2.1 Computational modeling

Numerical simulations using COMSOL version 4.2 Multiphysics with a drag force influence particle tracing module were conducted to analyze the lateral movement of particles under the influence of a centrifugal force field. Particle tracking module in COMSOL was used to track the particles in the asymmetric inertial channels (Zhang et al. 2013). This expression has a power law function form and is valid for spherical particles containing a wide range of particle Reynolds numbers (Re_p). Influence of Coriolis accelerations was also qualitatively studied by identifying dimensionless Rossby number (Ro), which is defined as the ratio of inertial to centrifugal forces. We confined the length of the channel to N-turns module depending on the rationale for modeling. These data were analyzed by the effect of centrifugal accelerations on particle trajectories as well as direction of rotation from computational model as this will determine the effect the Coriolis force will have on focusing of particles. Changes in x- and z-coordinates would give us information about module efficiency for particle focusing, and to this end, we modeled two different physical conditions to study the rotatory system and particle trajectory.

1. For rotational-geometric effects (Fig. 7i): Five consecutive x- and z-cut planes were set starting from A to E to study velocity contours due to the asymmetry of curvature in channels. For particle motion, F and G planes at 1.5 mm before and after passing the module, respectively. A single spherical PS particle having diameter 21 μm was introduced into F plane at some coordinates (x_F, z_F) and detected after passing the module to new point (x_G, z_G) on G plane (Fig. 7ii).
2. Lateral particle displacement and focusing in centrifugal field effects: An array of nine particles was used to identify computational behavior at different sections of the disc with two angular velocities with rotational direction control in Fig. 8. To qualitatively understand the effects the micromixer has on particle focusing and the Coriolis effect, a single particle was used with x- and y-plane predetermined initial positions. These sections consisted of 2-turn modules up to a total of 6 turns in Fig. 9. These computations were carried to better understand the effects of each component of particle effects by the rotational system. As it was previously mentioned, pressure gradients in rotating systems and their spin direction affect how the fluid behaves and thus interacts with the microchannel walls.

3.2.1.1 Physical settings Three-dimensional steady-state Navier–Stokes equation stationary model was used. Material and properties of the fluid were water. Mesh configuration was set to physics-controlled with size marked as normal with triangular elements; however, a trapezoid type was used at complicated boundaries. In our 3D simulations, it was about 1.5×10^5–3.0×10^5 elements or nodes. Wall boundary conditions were set to "no-slip" except at rectangular inlet and outlet channels. Inlet and outlet boundary conditions were set to zero pressure. Centrifugal movement was inserted into simulations as volume forces:

$$\mathbf{F}\omega = \rho\boldsymbol{\omega}^2\mathbf{r} \tag{2}$$

$$\mathbf{F}_c = -2\rho\boldsymbol{\omega} \times \mathbf{v} \tag{3}$$

where $\mathbf{F}\omega$ is the centrifugal force, $\mathbf{F}_c$ is the Coriolis force, ρ is the fluid density, $\boldsymbol{\omega}$ is the angular frequency of rotation, $\mathbf{v}$

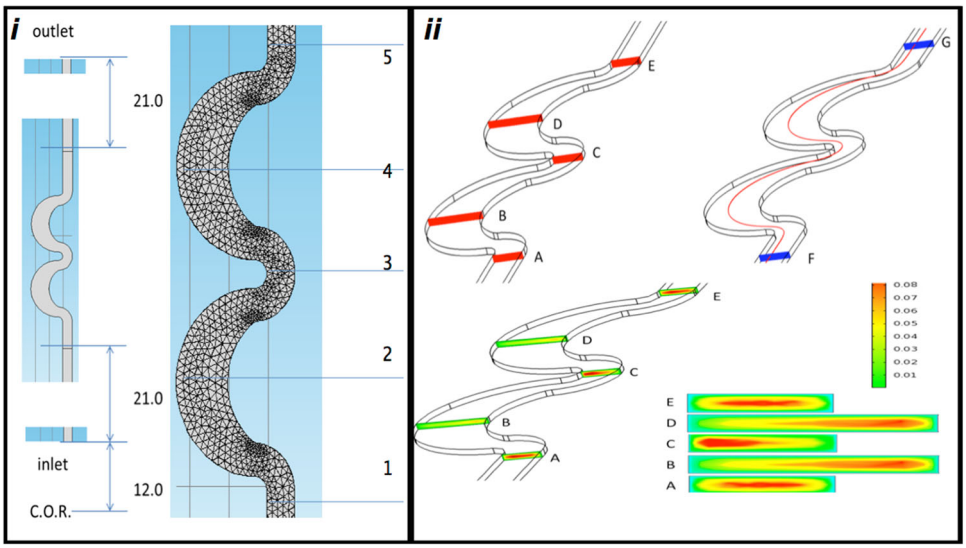

Fig. 7 Geometry definitions of computational simulations, **i** *x–y* plane view in cartesian coordinates demonstrating 2-turn module and 3D mesh quality used to describe flow field with 5 *x–z* cut planes representing equivalents in *A–E* in *top left*. **ii** *Top right* shows particle tracing methodology (*F–G*) (*thin red line*). *Bottom center* velocity profiles for counterclockwise rotation with frequency of 9 Hz. Profiles in straight channel sections (*A*, *E*) show homogeneous conditions, while *B* and *D* sections show higher velocity in direction of rotation. Section *C* shows a higher velocity gradient in direction of pressure gradient, which is a consequence of Coriolis force opposing direction of rotation (color figure online)

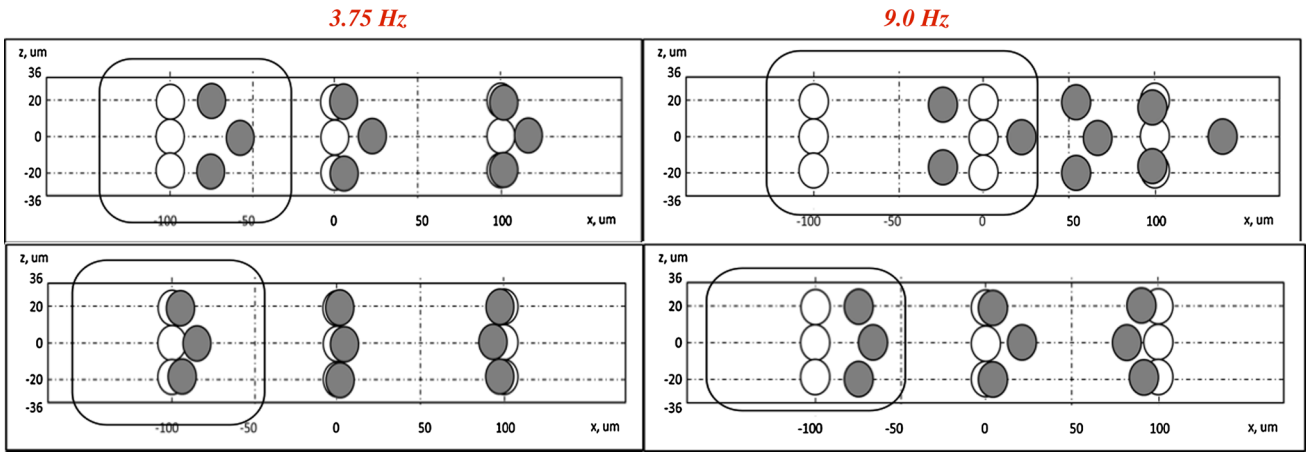

Fig. 8 *2-turn module* Tracing of 9 particles from F plane (*open circles*) to G plane (*gray circles*). *Top* direction of focusing. *Bottom* opposite direction of focusing. Rotational direction influences particle displacement greatly (see enclosed areas) suggesting spin direction of disc and translational movement in asymmetric channels confluence to produce particle focusing

is the fluid velocity. These expressions were adapted for *x*- and *y*-force components to Cartesian plane as follows:

$$\mathbf{F}_x = \rho\omega^2 x + 2\rho\omega \mathbf{r} v \tag{4}$$

$$\mathbf{F}_y = \rho\omega^2 y - 2\rho\omega \mathbf{r} u \tag{5}$$

$$\mathbf{F}_z = 0 \tag{6}$$

where u and v are the *x*- and *y*-fluid velocity components, respectively, $\mathbf{r} = \{-1, +1\}$ is the parameter determining the direction of rotation of disc, while there is no movement onto the *z*-axis.

3.2.1.2 Geometry Parallelepiped channel (length 60 mm; width 0.35 mm; depth 0.072 mm) was inserted into Cartesian geometry (Fig. 1i). It was supposed that center of rotation (C.O.R.) coincides with origin point (0, 0, 0). Left side of channel was chosen as inlet and right one as outlet. Inlet was located at 12 mm from origin point, i.e., rectangular inlet center of symmetry had the coordinates (0, 12, 0.036) to reproduce actual experimental conditions. Outlet plane center was at (0, 72, 0.036) correspondingly. The limiting factor has been shown to be fluidic resistance (Gossett and Di Carlo 2009), and to maintain it, we kept

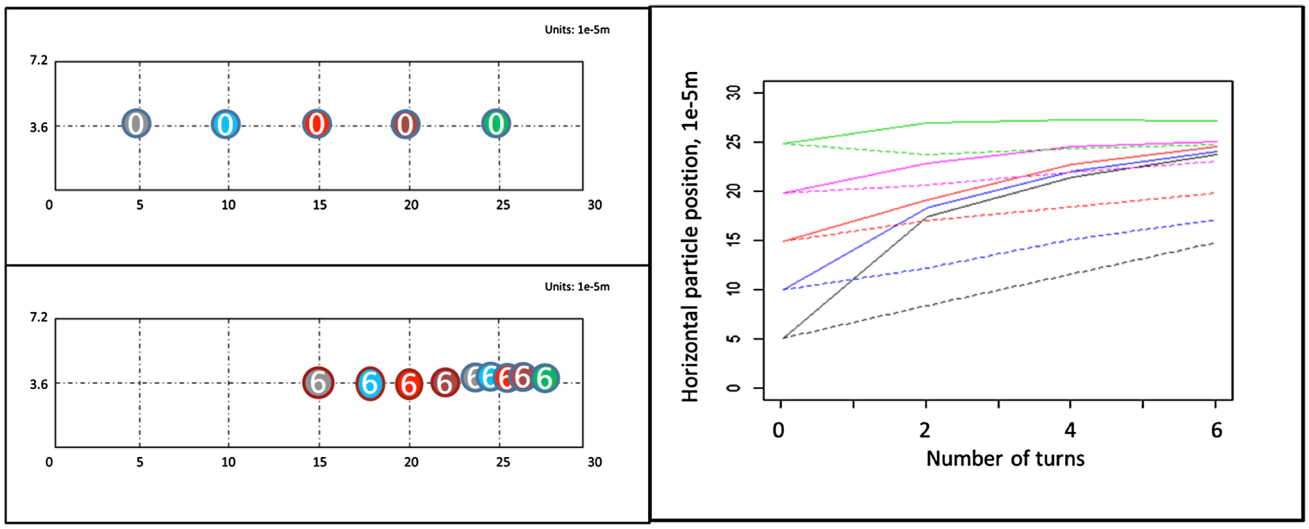

Fig. 9 *Top left side* view of cross-sectional area of microchannel with particle tracking with five different initial positions within channel and representative colors. *Bottom left* final lateral particle distance with Coriolis forces inactive (*red outer circle*) and active (*gray outer circle*) in a 6-turn module. *Right-side graph* demonstrating distance travelled of particles with Coriolis forces active (*solid lines*) and inactive Coriolis (*dashed*). *Line colors* match initial position colors. Notice inflection of particle trajectory closest to wall (*green*) demonstrating the effect of inertial wall effect–Coriolis force equilibrium (color figure online)

actual experimental length. But a segment of parallelepiped channel equal in length to the *2-turn module* was replaced in the middle of the channel symmetrically as it is shown on Fig. 7i for representative studies. All dimensions were kept the same.

3.2.1.3 Data analysis All computations were done in 3D Comsol module. The fluid simulation was solved with angular velocities set to 3.75 and 9 Hz, where specified, in the rotational platform module to identify threshold of influence of Coriolis force. Velocity profiles were measured with the use of five cuts along x- and z-plane as is demonstrated on Fig. 7ii *top left*: planes A and E correspond to 0.2 mm distance from end points of active area of simulation, respectively. Planes B and D correspond to widest cross sections of the module, and C plane is the smaller radius of asymmetric curved channels. Sectioning active principle fluidic region allows for easier study of the behavior of particle–fluid interactions. While in Fig. 7ii, *top right* demonstrates the trajectory of a single particle under same conditions. The inhomogeneity of velocities in specific regions of the 2-turn module is demonstrated in Fig. 6ii *bottom*. The velocity profile in straight channel segments A and E demonstrate a more uniform distribution in x-direction, less uniform in vertical z-direction classified as "classical" behavior and is well known in microfluidic channels. While for curved sections, the velocity profile inside the module cross sections is significantly non-uniform. This simulation stipulates the theory that this is the physical operating principle to change particle trajectories, especially in horizontal x-direction. Flow structure in our system, rotating curved channels, is very complex in nature as Coriolis and Dean transverse differential pressure gradients behave differently depending on various parameters (Sharma and Nandakumar 1995).

The velocity gradient in C plane forces the flow to behave like a pump. This can be clearly recognized from Fig. 7ii. The channel asymmetry causes velocity gradients moving radially downstream and creates sectional velocity fluxes. It is suggested this is due to the constriction where a necessary mass conservation argument produces a gradient to oppose the increased pressure at the smaller curved cross-sectional area while relaxing at the larger one. Curved channels are known to perturb flowing particles to equilibrium positions and interact with drag forces in secondary flows. How this affects the secondary Dean flows and drag, and to what magnitude it is not well understood (Humphry et al. 2010). The picture is very complicated with Dean flows used for lateral particle movement while particle focusing requires a balance of lift to drag forces in secondary flows. A clockwise velocity gradient did not show much different behavior (data not shown) reenforcing our argument.

To understand the effect of disc directional spin on particle movement, we studied the displacement of a 9-particle array at two frequencies as it is demonstrated in Fig. 8. This condition is representative of the cell–bead complexes entering the inertial unit in our experimental section Fig. 2e. The complexes enter the next unit closer to the equilibrium wall for focusing. In an effort to clarify and separate the influence of channel symmetry with innate centrifugal field effects, we employed sign

convention in Eqs. 4 and 5. Both a counterclockwise and clockwise rotation with frequencies of 3.75 and 9 Hz were chosen and found adequate from our previous experiments (Kitsara et al. 2013) for control of particle behavior with varying Coriolis force. The rectangular areas encompassing the circles show the influence on lateral movement between Coriolis forces and Dean secondary flows. The effect can be simplified by understanding that in these results, we identify the change in spin direction can distort the picture significantly. Obviously, this is Coriolis effect: if direction of F_c "coincides" with channel asymmetry, both factors work to concentrate particles closer to the right wall; otherwise, F_c compensates channel asymmetry and particles are not displaced significantly restricting more focusing in the central area of the channel.

A previous argument made (Gossett and Di Carlo 2009) was that this inward migration was stronger and contrary to the innate centrifugal effect in non-rotating curved channels, consistent with the theoretical argument made by Asmolov (1999). From our results, we identify that the effect is stronger with both the frequency and spin direction of the rotational system. To note, Khan–Richardson formulation uses difference in speeds between fluid flow and particle flow represented mainly as a drag force. We can think of them as Newtonian mass objects going across the channel but with fluidic resistance preventing their free motion.

Consistent with the previous published work (Gossett and Di Carlo 2009; Humphry et al. 2010), Fig. 9 shows that particle focusing in inertial curved microfluidics is dependent on initial z-coordinate position of particle, the *more to the center of channel, more acute the effect is.* This is proven with the experimental results of particle entrainment leading to complex focusing at lower speeds. Individual particles were placed at specific x- and y-coordinates and trajectories tracked with Coriolis force turned on or off by the use of Eq. 3. Tracing of particles under active Coriolis force (solid lines) follows sequentially decreasing slope trajectories entering every 2-turn module, while the particle closest to the focusing wall has the least pronounced slope. The translational movement of the particle is linear when the Coriolis force is deactivated (not a real physical system), with the exception of the one nearest the wall where focusing will occur (dashed lines). This shows that particle displacements are more dramatic for initial positions closer to the right wall.

Noticing the behavior of the particle nearest to side of wall focusing in both cases, it seems to have inverse mirror trajectories. When Coriolis forces are not active, complex 3-dimensional numerical simulations show wall effect to be the dominant force in the system. This cannot be proven in a real experimental setup, however, but it allows for qualitative understanding of a more complex interaction of forces in a rotating system due to physical relationships resulting from calculated Rossby number value of $Ro \ll 1$, a condition where Coriolis forces are dominant and convective inertial effects are small. The Reynolds number under our radial velocity is greater than unity, suggesting that viscous interactions between the wall and the fluid may not be as strong under this fluid flow. However, how this affects the generation of turbulence or vortices interacting with secondary flows in curved channels, such as the Ekman boundary layer, which is quite complex and not well understood (Sharma and Nandakumar 1995) The Ekman number in our system demonstrates the Coriolis force is dominant over viscous forces.

Additionally, the Dean drag force is responsible for providing translation of particles to the final equilibrium position in curved channels (Kuntaegowdanahalli et al. 2009) and it scales with average velocity squared. The contractions and expansions of the asymmetric channel lead to nonlinear shear flow and affect the local velocity gradient. Dean forces in curved rotating channels demonstrate that secondary flows are composed of (1) the secondary flow due to the curvature effects of the centrifugal force; (2) the secondary flow due to the rotation (effects of the Coriolis force), which is enhanced due to the rotating system. Fluid cells with counter rotating vortices are developed on top and bottom near channel walls, where the shear rate gradient is highest. This is known as the Ekman layer. In a curved rotating channel, this interaction is highly complex and not well understood.

We suggest a theoretical mechanism for why the green particle remains trapped closer to the wall further into the region of high viscous forces. Viscous stresses determine drag force and also vorticity. This flow affects particle position in addition to the lift force; however, the Dean drag force affects these fluid cells and pushes them toward the inner wall where they focus and are balanced by viscous drag force. The balance subjecting the particles to the equilibrium position into the secondary vortices (Gossett and Di Carlo 2009; Kuntaegowdanahalli et al. 2009) is, in our computations, dominant due to the initial particle position and momentum increase obtained as it travels from third to fifth turns providing enough velocity for the particle to find a new balance closer to the wall. Here, it becomes trapped by the viscous force (Hogg 1994) or drag force component. The work above makes an important assumption that wall lift effects are not important to balancing Dean drag. This is demonstrated with the same particle position (dashed green) with the Coriolis force turned off and thus the Ekman layer is not present. It demonstrates that the particle does reach the same equilibrium position without the aid of Coriolis force, but does not reach into the region of high viscous force as it is not

aided by the pressure gradient. However, this area needs more sophisticated numerical simulation to assess the complete mechanism.

4 Conclusion

An integrated system for the advancement of lab-on-chip toolbox was designed and demonstrated. A first of its kind, the prototype consists of two units. Both samples, spiked blood with cancer cells and epitope covered bead samples, are loaded in a single step prior to the start of the centrifugal spinning protocol. A mixing unit for the incubation of MCF7 cancer cell line with PS beads functionalized with its respective epitope and an inertial flow field unit with focusing secondary flows to determine the binding efficiency of cancer cells of the system are placed in line without the use of any external forces. The system utilized single flow rate on both units. Architectural design of both systems enabled high efficiency statistics by the exploitation of centrifugal system forces where they provide an advancement to systems developed previously.

This system provides the following advantages over pump-driven system:

1. Enhancement of binding by mixing of cancer cells to particles in Dean channels. The centrifugal field provides this enhancement, and the term "flipping" was the descriptive term, over a pressure- or pump-driven system where it does not exist.
2. Complex formation leads to the ease of cancer cell identification without sophisticated detection equipment and eliminates the need of off-chip sample handling.
3. The buoyancy in transversal movement of particles in the azimuthal direction is overcome while particles are under constant centrifugal force; its effect is eventual partial sedimentation. This allows the complex to align and enter the inertial channel closer to the flow-focusing wall.
4. Ability of particles with different densities to separate due to enhanced sedimentation in the inertial unit is not available in a pressure system (Oakey et al. 2010; Gossett and DiCarlo 2009; Asmolov 1999). However, in a previous work, we describe this enhancement.

High efficiency was obtained with 2 % v/v blood but decreasing degree of binding and focusing resulting with increased blood content. Though the system is reliable and efficient, a blood fractionation such deterministic lateral displacement (DLD) unit would render binding and separation results similar to those with off-chip incubation (baseline). Due to the low number of cells processed, this integrated system can in principle be utilized for CTC identification and capture. Though this is a positive selection method, any epitope covered bead can serve for the detection of specific cancer cells that can be expanded to cells with non-epithelial origin as well as a secondary line for negative selection by exploiting sedimentation forces of varying microparticle densities.

Acknowledgments Authors would like to thank Dr Macdara Glynn for supplying MCF7 cells. This material is based upon works supported by the Science Foundation Ireland under Grant No. 10/CE/B1821.

References

Abaxis.com. Accessed May, 2013

Asmolov E (1999) The inertial lift on a spherical particle in a plane Poiseuille flow at large channel Reynolds number. J Fluid Mech 381:63–87

Boubnov BM, Golitsyn GS (1995).Convection in rotating fluids. Springer, Berlin, p 8. ISBN: 0-7923-3371-3

Brenner T, Glatze T, Zengerle R, Ducree J (2005) Batch-mode mixing on centrifugal microfluidic platforms. Lab Chip 5:146–150

Burger R, Ducree J (2012) Handling and analysis of cells and bioparticles on centrifugal microfluidic platforms. Expert Rev Mol Diagn 12:407–421

Capretto L, Cheng W, Hill M, Zhang X (2011) Micromixing within microfluidic devices. Top Curr Chem 304:27–68

Chen G, Albertsa C, Rodriguez W, Toner M (2010) Concentration and purification of human immunodeficiency virus type 1 virions by microfluidic separation of superparamagnetic nanoparticles. Anal Chem 82:723. doi:10.1021/ac9024522

Cho YK, Lee JG, Park JM, Lee BS (2007) One-step pathogen specific DNA extraction from whole blood on a centrifugal microfluidic device. Lab Chip 7:565–573

Fang W, Yang J (2009) A novel microreactor with 3D rotating flow to boost fluid reaction and mixing of viscous fluids. Sens Actuators B Chem 140:629–642

Godino N, Gorkin R III, Linares AV, Burger R, Ducree J (2013) Comprehensive integration of homogeneous bioassays via centrifugo-pneumatic cascading. Lab Chip 13:685

Gossett D, Di Carlo D (2009) Particle focusing mechanisms in curving confined flows. Anal Chem 81:8459–8465

Hansson J, Karlsson J, Haraldsson T, Brismar H, van der Wijngaart W, Russom A (2012) Inertial microfluidics in parallel channels for high-throughput applications. Lab Chip 12:4644–4650

Hogg AJ (1994) Inertial migration of a non-neutrally buoyant particle in a two-dimensional shear flow. J Fluid Mech 272:285–318

Hong CC, Choi J-W, Ahn CH (2004) A novel in-plane passive microfluidic mixer with modified Tesla structures. Lab Chip 4:109–113. doi:10.1039/B305892A

Hou HW, Bhagat AAS, Lee WC, Huang S, Han J, Lim CT (2011) Microfluidic devices for blood fractionation. Micromachines 2:319–343. doi:10.3390/mi2030319

Humphry K, Kulkarni P, Weitz D, Morris J, Stone J (2010) Axial and lateral particle ordering in finite Reynolds number channel flows. Phys Fluids 22:081703

Joseph DD (2002) Power law correlations for the lift force on a particle in plane Poiseuille flow DDJ/2002/papers/Wang-PLCorr/nt_lift.doc

Jung JH, Kim GY, Seo TS (2011) An integrated passive micromixer–magnetic separation–capillary electrophoresis microdevice for

rapid and multiplex pathogen detection at the singlecell level. Lab Chip 11(20):3465–3470. doi:10.1039/c1lc20350a
Kamholz A, Weigl B, Finlayson B, Yager P (1999) Quantitative analysis of molecular interaction in a microfluidic channel: T-sensor. Anal Chem 71:5340–5347
Kirby D, Siegrist J, Kijanka G, Burger R, Sheils O, O'Leary J, Ducrée J (2012) Centrifugo-magnetophoretic particle separation. Microfluid Nanofluid. doi:10.1007/s10404-012-1007-6
Kitsara M, Aguirre G, Efremov V, Ducree J (2013) Lab-on-a-disc platform for particle focusing induced by inertial forces. In: Proceedings of SPIE 8765, Bio-MEMS and Medical Microdevices 87650R. doi:10.1117/12.2017438
Kuntaegowdanahalli S, Bhagat S, Kumarb G, Papautsky I (2009) Inertial microfluidics for continuous particle separation in spiral microchannels. Lab Chip 9:2973–2980
La M, Park SJ, Kim HW, Park JJ, Ahn KT, Ryew SM, Kim DS (2013) A centrifugal force-based serpentine micromixer (CSM) on a plastic lab-on-a-disk for biochemical assays. Microfluid Nanofluid 15:87–98. doi:10.1007/s10404-012-1127-z
Levin S, Giddings J (1991) Continuous separation of particles from macromolecules in split-flow thin (SPLITT) cells. J Chem Tech Biotechnol 50:43–56
Lu L, Ryu K, Liu C (2002) A magnetic microstirrer and array for microfluidic mixing. J Microelectromech Syst 11:462–469
Matas J, Morris J, Guazelli E (2009) Lateral force on a rigid sphere in large-inertia laminar pipe flow. J Fluid Mech 621:59–67
Morijiri T, Hikida T, Yamada M, Seki M (2010) Microfluidic counterflow centrifugal elutriation system for sedimentation-based cell separation. 978-0-9798064-3-8/μTAS 2010/$20©2010 CBMS
Morijiri T, Sunahiro S, Senaha M, Yamada M, Seki M (2011) Sedimentation pinched-flow fractionation for size- and density-based particle sorting in microchannels. Microfluid Nanofluid 11:105–110
Mugele F, Baret JC (2005) Electrowetting: from basics to applications. J Phys Condens Matter 17:R705–R774
Noroozi Z, Kido H, Micic M, Pan H, Bartolome C, Princevac M, Zovaland J, Madou M (2009) Reciprocating flow-based centrifugal microfluidics mixer. Rev Sci Instrum 80:075102
Oakey J, Applegate R Jr, Arellano E, Carlo DD, Graves S, Toner M (2010) Particle focusing in staged inertial microfluidic devices for flow cytometry. Anal Chem 82:3862–3867
Pappas D, Wong K (2007) Cellular separations: a review of new challenges in analytical chemistry. Anal Chim Acta 601:26–35
Paterlini-Brechot P, Benali L (2007) Circulating tumor cells (CTC) detection: clinical impact and future directions. Cancer Lett 253:180–204
Schaff U, Sommer G (2011) Whole blood immunoassay based on centrifugal bead sedimentation. Clin Chem 57:753–761
Sharma R, Nandakumar K (1995) Flow through rotating rectangular ducts. Phys Fluids 7:1568–1575
Siegrist J, Gorkin R, Bastien M, Stewart G, Peytavi R, Kido H, Bergeron M, Madou M (2010) Validation of a centrifugal microfluidic sample lysis and homogenization platform for nucleic acid extraction with clinical samples. Lab Chip 10:363–371
Sollier E, Rostainga H, Pouteaua P, Fouilleta Y, Achard JL (2009) Passive microfluidics devices for plasma extraction from whole human blood. Sens Actuators B Chem 141:617–624
SpinDx. http://www.sandia.gov/biosystems/docs/spindx.pdf
Stott SL, Toner M et al (2010) Isolation of circulating tumor cells using a microvortex generating herringbone chip. PNAS 107:18392–18397
Stroock A, Dertinger S, Ajdari A, Mezic I, Stone H, Whitesides G (2002) Chaotic mixer for microchannels. Science 295:647
Sudarsan AP, Ugaz V (2006) Multivortex micromixing. PNAS 103(19):7228–7233
Tibbe A, Miller M, Terstappen L (2007) Statistical considerations for enumeration of circulating tumor cells. Cytom A 71:154–162
Tsai H Jr, Lin L (2002) Active microfluidic mixer and gas bubbler driven by thermal bubble micropump. Sens Actuators A Phys 97:665–671
Vijayendran R, Motsegood K, Beebe D, Leckband D (2003) Evaluation of a three-dimensional micromixer in a surface-based biosensor. Langmuir 19:1824–1828
Voldman J, Gray J, Schmidt J (2000) An integrated liquid mixer/valve. Microelectromech Syst 9:295–302
Wang H, Iovenitti P, Harvey E, Masood S (2002) Optimizing layout of obstacles for enhanced mixing in microchannels. Smart Mater Struct 11:662
Wong S, Ward M, Wharton C (2004) Micro T-mixer as a rapid mixing micromixer. Sens Actuators B 100:365–385
Xin W, Chen X, Mab X, Kong X, Xua Z, Wang J (2011) Fast DNA hybridization on a microfluidic mixing device based on pneumatic driving. Talanta 84:565–571
Yang Z, Matsumoto S, Goto H, Matsumoto M, Maeda R (2001) Ultrasonic micromixer for microfluidic systems. Sens Actuators A Phys 93:266–272
Zhang J, Guo Q, Liu M, Yang J (2008) A lab-on-CD prototype for high-speed blood separation. J Micromech Microeng 18:125025
Zhang J, Li W, Li M, Alici G, Nguyen N-T (2013) Particle inertial focusing and its mechanism in a serpentine microchannel. Microfluid Nanofluid. doi:10.1007/s10404-013-1306-6